DOI:10.1190/segam2019-3200118.1

Reflectivity decomposition: theory method, synthetic example and application in the Midland Basin

Chen Liang, Lumina Technologies, Inc.; John Castagna, University of Houston; Marcelo Benabentos, CNOOC*

Summary

Conventional sparse-spike seismic inversion can have difficulty characterizing layers with weak reflectivity that are interfering with side-lobes from immediately overlying or underlying large reflection events. The inversion parameterizations and constraints are dominated by large reflections and may result in inversion instability for weak events that are "smothered" by the stronger reflections. Any seismogram can be decomposed according to the size of inverted reflection coefficients producing the seismogram. Reflection coefficients can be sorted by their magnitude and sign and new seismic traces can be created including only reflection coefficients within certain amplitude ranges. Large inverted reflection coefficients can be removed and the residual reinverted, thereby stabilizing inversions for the remaining weak events. By this reflectivity decomposition, subtle impedance variations occurring in the vicinity of nearby strong reflections can be revealed seismically. This approach is demonstrated on a 3D seismic dataset in the Midland basin. Amplitude maps for weak events are stabilized such that previously undetectable porous intervals can be detected, mapped, and correlated to well logs.

Introduction

Seismic inversion non-uniqueness can be constrained with prior information (Tarantola, 2005). The attempt to eliminate implausible solutions, however, does not guarantee the inversion results will be necessarily close to the correct solution. Liang and Castagna (2017) explain the limited resolving ability inherent in sparse inversions and show that inverse results would deteriorate when earth structure is complicated. Zhang and Castagna (2011) use thin-layer reflectivity patterns in order to resolve more details in the seismic data; however, the non-uniqueness issue in the inversion may still be severe especially when reflection are interfering with each other. The situation becomes even more unfavorable for small events which are covered up by dominate strong reflections. It is desirable to remove such interferences to limit distortion of seismic responses of zones of interest. Deconvolution can at best compress the wavelet and interference may remain. Objective functions in seismic inversion can be dominated by strong events and be less pristine about preserving the character of weak events. A correct inversion for such small reflections is thus unlikely to be achieved on the original seismic data, regardless of how the inversion is regularized. It has been a long-standing and neglected problem in seismic reflectivity inversion that those events that are subtle and hidden but truly relevant to zones of interest have not been properly inverted.

We propose that the inverted reflectivity can be sorted by their amplitudes and used to recreate new reflectivity series with only reflection coefficients within certain amplitude ranges. Such an operation of dividing a reflectivity sequence into separate components is referred to as ***reflectivity decomposition***. Obviously, stronger reflections are more likely than relatively weak reflections to be correctly inverted given proper regularizations. Having the accurate seismic responses separated from the rest of the seismic trace can thus restore those subtle amplitudes that are hidden in the original data, resulting in zones of interest, if any, to be revealed in the weak seismic trace. This allows inversion for the reflection coefficients of small strength in a more robust manner. We present a strategy dealing with the issue by decomposing seismic traces by reflection amplitude and reinverting the reflectivity-decomposed traces. A practical implementation procedure of the reflectivity decomposition is summarized. We employ a single-trace synthetic example to demonstrate the effectiveness of the method. A field data example from the Midland basin suggest that target visualization has been largely enhanced in the studied interval. The reflectivity-decomposed results produced by the method are validated by a quantitative analysis involving multiple wells.

The methodology

The basic assumption for reflectivity decomposition is that the seismic trace $s(t)$ is produced by convolution between a stationary seismic wavelet $w(t)$ and the reflectivity series $r(t)$, with random noise $n(t)$ added:

$$s(t) = w(t) * r(t) + n(t) . \quad (1)$$

For sparsity in the reflectivity solution, the inverted result is assumed to possess a prior distribution that is exponentially tapered, based on which an objective function can be derived to be optimized:

$$\min[\| d - Gm \|_2 + \lambda \| m \|_1] . \quad (2)$$

where $\boldsymbol{d}$ is data vector, $\boldsymbol{m}$ represents model parameters, $\boldsymbol{G}$ is kernel matrix, λ is regularization parameter. The L1-norm global optimization can be achieved using a variety of approaches (Oldenburg et al., 1983; Sacchi, 1997; Taylor et al., 1979). We use the basis-pursuit principle (Chen et al.,

10.1190/segam2019-3200118.1

DOI:10.1190/segam2019-3200118.1

2001) to accomplish the sparse-spike inversion. The kernel matrix is comprised of time-shifted wavelets and we invert for their weights.

To simplify, we assume a noise-free seismogram and a well-established wavelet. An inverted reflectivity series that reproduces the original seismic trace can be obtained by iteratively applying the sparse inversion that is properly regularized. Suppose that strong and weak components in the true and inverted reflectivity are represented by $rf_{trus}(t)$, $rf_{truw}(t)$, $rf_{invs}(t)$ and $rf_{invw}(t)$, respectively. The equality is thus as followed:

$$rf_{trus}(t) * w(t) + rf_{truw}(t) * w(t) = rf_{invs}(t) * w(t) + rf_{invw}(t) * w(t) \quad (3)$$

Although being not identical due to non-uniqueness, wavelet error, discretization, etc., strong inverted reflection coefficients are presumed to be well restored to the extent that the corresponding seismic response coincides with that of the strong component in the true reflectivity. Removing the nearly equivalent strong reflection terms, the seismic response of inverted small reflection coefficients is thus approximately equal to that of the small ones in the true reflectivity.

$$rf_{invw}(t) * w(t) \approx rf_{truw}(t) * w(t) . \quad (4)$$

This implies that, although weak reflection coefficients may be corrupted in the original inversion, they possess similar response in the wavelet band and the true weak reflectivity may be well recovered as the reflectivity-decomposed trace is re-inverted with new constraints.

Practical implementation procedure

A practical procedure of implementing the reflectivity decomposition method is suggested below:
1) A post-processing seismic volume that has sufficiently high signal-to-noise ratio is required to accomplish the reflectivity decomposition.
2) Data conditioning, e.g. bandpass filtering can be employed accordingly if applicable.
3) Original matches between well-log synthetics and seismic data are important to validate the reflectivity-decomposed results and allow quantitative interpretation.
4) Employ a robust sparse inversion algorithm. The proper regularization parameters can be determined based upon the criterion that seismic magnitudes are tied to the corresponding responses from well logs after the inverted strong spikes are eliminated.
5) Given a volume of inverted reflection coefficients, those within each zone of interest are collected to construct histograms and can be reduced in fractions of standard deviation with only small ones remaining. The reflectivity-decomposed results are calibrated to simultaneously satisfy all usable wells in the survey while the number of strong spikes to be thrown away is maximized.
6) The small reflection coefficients that are passed are re-convolved with the seismic wavelet and the events are re-inverted. Desired reflector patterns can be user-defined and selected out by simple matching pursuit (Mallet and Zhang, 1993).
7) The reflector pairs resulting from the reflection coefficients that are re-inverted from the reflectivity-decomposed traces can be reshaped by the desired wavelet. Data reconditioning may be needed to suppress amplified noise.

Synthetic example

The original reflectivity series is composed of various groups producing seismic events for which a small reflector is covered up by the large reflection event nearby (Figure 1a). Convolving with a limited-band wavelet, Figure 1b is the original seismic trace in which those weak events have become indistinct and been confused with the strong reflections. As a result, a direct sparse inversion produces inverted reflectivity series of which the large spikes have been properly recovered while those small satellite reflectors, however, are unidentifiable (Figure 1c). By reflectivity decomposition, the inverted reflection coefficients are separated into a series (Figure 1d) with only large magnitudes and the other (Figure 1e) with only small ones. The original seismogram can thus be divided into separate components (Figure 1f and 1g) which are simply generated by reconvolving the corresponding reflection coefficients with the seismic wavelet. The benefit is that the disordered and unpleasing parts in the original inverted result have been restored in the wavelet-reconvolution trace after the correctly inverted spikes are removed, because of linear additivity in the convolution operation. Reinverting the weak reflectivity-decomposed seismogram thus has had the weak reflection coefficients well resolved (Figure 1h), compared to the true small reflectivity (Figure 1i).

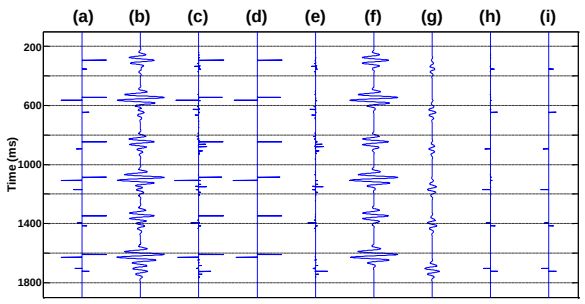

Figure 1: a) Original reflectivity; b) original seismogram; c) original inverted reflection coefficients; d) strong reflectivity component; e) weak reflectivity component; f) strong component in seismic response; g) weak component in seismic response; h) inverted reflectivity of weak seismic trace – compare to original inverted weak reflectivity (e); i) original weak reflectivity.

Real data application

The real dataset is located in the Midland basin that is part of the larger Permian basin (Hill, 1984; Frenzel et al., 1988). Subsidence of the Midland basin led to the deposition of the carbonate formations Canyon, Cisco and vertically accreting pinnacles. The overlying Wolfcamp Shale provides top and lateral seals for these units. The Cisco and Canyon interval is characterized by low impedance porous zones that are seismically thin layers. The prospectives are covered up by the large impedance contrast interface across the clastic-carbonate boundary as well as any considerable lithological change in the carbonates. Those reflection interferences are prone to obscure the interpretation of the zones of interest, which however, are to be ameliorated and resolved by using the reflectivity-decomposition technique.

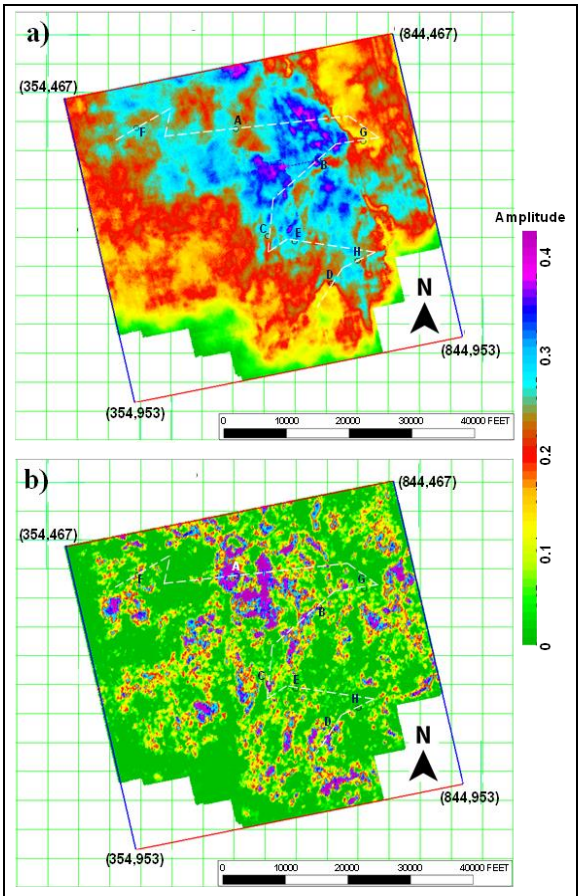

Figure 2: Amplitude maps (a) original data; (b) reflectivity-decomposed inversion result. The arbitrary line through various well locations (marked A-H) is denoted by white dash line.

Figure 2 shows the RMS amplitude maps extracted from the studied interval before and after the procedure is implemented. The subtle impedance variation caused by high porosity hidden in the original data have been revealed and mapped geologically (Figure 2b). The spotty features representing the desired seismic response in the result are quite distinct as compared to the cloudy map computed from the original data where the amplitudes are spatially averaged by strong interfering reflections (Figure 2a).

Figure 3a exhibits the vertical section extracted along the arb line (white dashed in Figure 2) from the original seismic volume in which those targets are indiscernible and hidden beneath the strong overburden reflection. After separating reflection coefficients, wavelet reconvolution, and spike re-inversion, the interfering events are eliminated. The otherwise indistinct amplitudes are highly anomalous on the resulting section (Figure 3b); only events with trough-over-peak response indicative of porosity appear as this desired reflector pattern has been selected. The reflectivity-decomposed results can be validated by a quantitative analysis between usable wells in the survey. In this case, we compute average porosity and layer thickness for porous intervals at each well. Another layer property that is the product of porosity and thickness is calculated as well. Before and after the method is applied, seismic RMS amplitudes are computed accordingly for each zone of interest.

The average porosity and the product of porosity and thickness are cross-plotted versus the seismic amplitude, respectively (Figure 4a and 4b). There is no apparent correlation between seismic amplitude and either of the layer properties in the original data (blue circles). However, those scattered circles have been redistributed in the reflectivity-decomposed inversion results (red circles). For the rock porosity alone (Figure 4a), some general trend occurs that the average porosity increases with increasing amplitude, appearing however to indicate two different geological trends. For the porosity times thickness (Figure 4b), the scatter has been greatly reduced, and a linear trend consistent with expectations materializes; the brighter the seismic response, the greater the porosity times thickness. This combined property provides a useful quantity that is important for volumetrics determinations, because porosity and thickness both effect the seismic amplitude for thin layers but multiplying them mitigates the tuning effect.

To investigate statistical significance of the correlations (*f*-test) for the crossplots, a simple linear model is assumed and the seismic amplitude is selected as the variable used to predict the layer properties (Fisher, 1925; Snedecor, 1989). Generally, the correlation coefficient for each layer property has been largely increased in the reflectivity-decomposed inversion result. Most importantly, the correlation to seismic amplitude for the reflectivity-decomposed inversion result and the statistical significance (an *f*-test value of 97.77) of that correlation (a correlation coefficient of 0.96) are particularly excellent for the porosity-times-thickness case.

Reflectivity decomposition

The direct porosity prediction, though less favorable, is still good (a correlation coefficient of 0.84) and of high statistical significance (an *f*-test value of 19.57).

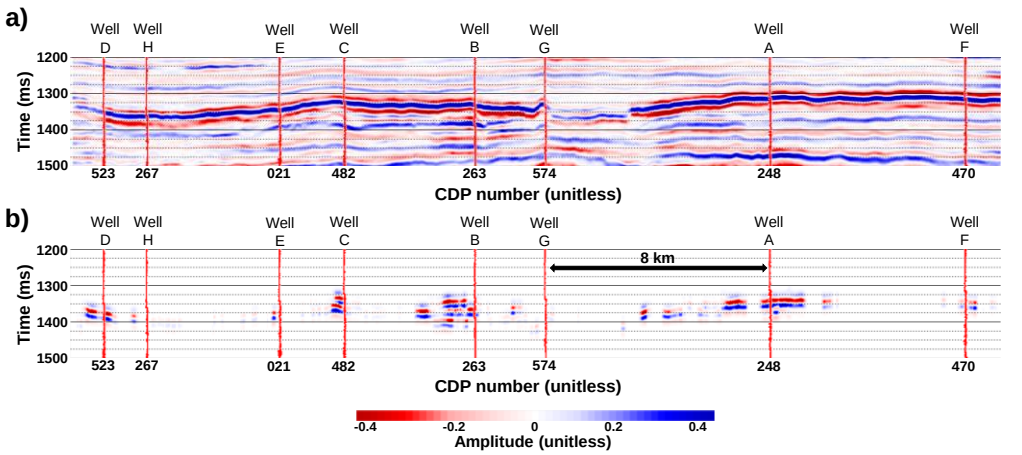

Figure 3: Cross sections extracted along the arbitrary line from (a) original data and (b) reflectivity-decomposed inversion result. Well logs are inserted against the sections for reference.

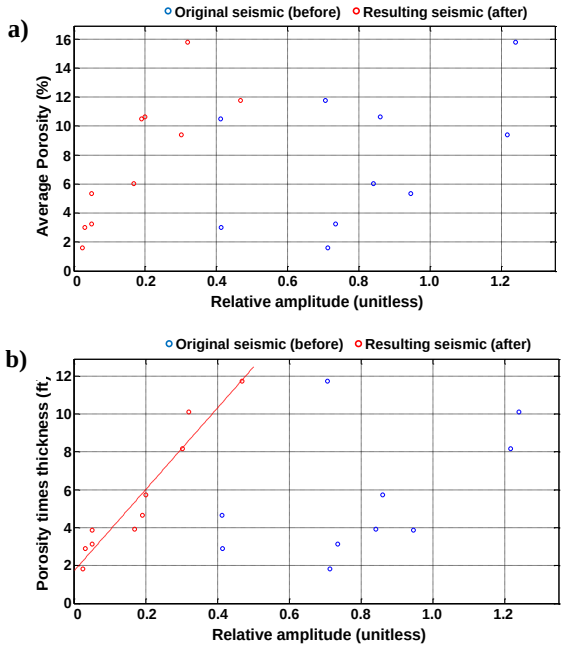

Figure 4: Crossplots of average porosity versus seismic amplitude (a) and porosity times thickness versus seismic amplitude (b). Original data is denoted by blue circles; result data is denoted by red circles.

Conclusions

Sparse-spike inverted reflection coefficients can be decomposed into separate components including ones within certain amplitude ranges. Subtle impedance anomalies hidden in original seismic data can be uncovered and illuminated on weak-reflectivity seismic responses. A single-trace example demonstrates that various weak events that are covered up by strong reflections nearby have been well resolved in the reflectivity-decomposed inversion result. The field data example shows that in the map view, distribution of porous zones has been revealed by the method; in the cross-section view, strong reflections are removed, interference is reduced and only events with desired trough-over-peak responses appear. Quantitative analysis suggests that reflectivity decomposition allows reflectors related to porosity development to be properly inverted and the extracted amplitudes from reflectivity-decomposed inversion correlate much better to porosity at wells than does the original data.

DOI:10.1190/segam2019-3200118.1

REFERENCES

Chen, S. S., D. L., Donoho, and M. A., Saunders, 2001, Atomic decomposition by basis pursuit: Society for Industrial and Applied Mathematics Review, **43**, 129–159, doi: https://doi.org/10.1137/S003614450037906X.

Fisher, R. A., 1925, Statistical methods for research workers: Oliver and Boyd (Edinburgh).

Frenzel, H. N., et al., 1988, The Permian Basin region, *in* L. L. Sloss, ed., Sedimentary cover North American Craton, U.S.: Geological Society of America **D-2**, The Geology of North America, 261–306.

Hills, J. M., 1984, Sedimentation, tectonism, and hydrocarbon generation in Delaware basin, west Texas and southeastern New Mexico: AAPG Bulletin, **68**, 250–267, doi: https://doi.org/10.1306/ad460a08-16f7-11d7-8645000102c1865d.

Liang, C., J. P., Castagna, and R. Z., Torres, 2017, Tutorial: Spectral bandwidth extension — Invention versus harmonic extrapolation: Geophysics, **82**, no. 4, W1–W16, doi: https://doi.org/10.1190/geo2015-0572.1.

Mallet, S., and Z., Zhang, 1993, Matching pursuits with time-frequency dictionaries: IEEE Transactions on Signal Processing, **41**, 3397–3415, doi: https://doi.org/10.1109/78.258082.

Oldenburg, D. W., T., Scheuer, and S., Levy, 1983, Recovery of acoustic impedance from reflection seismograms: Geophysics, **48**, 1305–1414, doi: https://doi.org/10.1190/1.1441413.

Sacchi, M. D., 1997, Reweighted strategies in seismic deconvolution: Geophysical Journal International, **129**, 651–656, doi: https://doi.org/10.1111/j.1365-246X.1997.tb04500.x.

Snedecor, G. W., and W. G., Cochran, 1989, Statistical methods, 8th ed.: Iowa State University Press.

Tarantola, A., 2005, Inverse problem theory and methods for model parameter estimation: SIAM.

Taylor, H. L., S. C., Banks, and J. F., McCoy, 1979, Deconvolution with the ℓ1 norm: Geophysics, **44**, 39–52, doi: https://doi.org/10.1190/1.1440921.

Zhang, R., and J. P., Castagna, 2011, Seismic sparse-layer reflectivity inversion using basis-pursuit decomposition: Geophysics, **76**, no. 6, R147–R158, doi: https://doi.org/10.1190/geo2011-0103.1.